PHYSICAL REVIEW A

ATOMIC, MOLECULAR, AND OPTICAL PHYSICS

THIRD SERIES, VOLUME 47, NUMBER 5 PART B MAY 1993

ARTICLES

Xe L and M x-ray emission following Xe^{44-48+} ion impact on Cu surfaces

M. W. Clark,* D. Schneider, D. Dewitt, and J. W. McDonald
Lawrence Livermore National Laboratory, University of California, Livermore, California 94550

R. Bruch
University of Nevada, Reno, Reno, Nevada 89557

U. I. Safronova and I. Yu. Tolstikhina
Institute of Spectroscopy, Russian Academy of Sciences, Troitsk, 142092, Moscow Region, Russia

R. Schuch
Manne Siegbahn Institute of Physics, S-10405 Stockholm, Sweden
(Received 24 April 1992)

The x-ray emission following the impact of highly charged Xe^{q+} ($q=44-48$) ions of 7-keV/q energy on a Cu surface has been measured. Theoretically we have derived an analytic formula which allows us to calculate the $2l$-nl', $3l$-nl', and $4l$-nl' ($n \leq 5$), L, M, and N x-ray transition energies averaged over spin and angular-momentum quantum numbers (L and S) as a function of the electron occupation numbers (k_i) for the states $Q = 1s_1^k 2s_2^k 2p_3^k 3s_4^k 3p_5^k 3d_6^k 4s_7^k 4p_8^k 4d_9^k 4f_{10}^k 5s_{11}^k 5p_{12}^k$. In accordance with our theoretical predictions the observed L x-ray structures shift toward higher energies and increase in intensity relative to the M x rays with increasing charge state. We have also observed an increase in high-energy satellite-line intensities with the increasing number of $2p$ vacancies. In calculating the radiative-transition probabilities we have found that the dominating electric-dipole transitions for L and M x rays are of the kind $2p$-$3d$ and $3d$-$4f$, respectively. A comparison between measured peak positions and calculated transition energies reveals that direct feeding by approximately 13 electrons can explain the main features of the observed x-ray emission spectra.

PACS number(s): 31.50.+w, 32.30.Rj, 79.20.Rf

I. INTRODUCTION

Much effort is presently directed towards research on ion-surface interactions using very highly charged ions [1]. This research became feasible with the development of new and advanced ion sources such as electron cyclotron resonance (ECR) sources, the electron-beam ion source (EBIS), and the electron-beam ion trap (EBIT) [2–6]. The EBIT is essentially very similar to an EBIS, except for the difference in the length of the electron-ion interaction path. Both ion sources use the principle of producing highly charged ions via successive ionization of atoms with intense energetic electron beams. The recently developed technique [2] to extract highly charged ions from the EBIT, which has been originally designed as an ion trap, allows the use of ions up to Th^{80+} for ion-surface interaction studies. These studies are mainly aimed at understanding the neutralization dynamics of highly charged ions as they approach the surface and penetrate into the solid. Such highly charged projectile ions carry up to several hundred keV potential energy and x-ray emission studies are particularly suited to illuminate the different interaction processes which lead to the transfer of this energy to the surface. Furthermore, such new experiments allow the observation of surface modifications induced by a medium-to-heavy ion impact. A more complete picture may eventually emerge from the simultaneous measurements of the Auger-electron and x-ray emission, sputter-ion yields, and the charge exchange of the projectile ions following the ion-surface in-

teraction [3–16]. X-ray emission has been measured with low resolution for $Ne^{9+,10+}$, $Ar^{17+,18+}$, and Kr^{36+} ion impact on surfaces. For the cases of Ne^{9+} and $Ar^{17+,18+}$ ions, high-resolution measurements using crystal spectrometers have been conducted. From these measurements the occurrence of "hollow atoms" during the neutralization process has been inferred [3]. Such superexcited states with nearly empty core levels are created mainly at small ion approach velocities where the ion-surface interaction is dominant. Multiple inner-shell vacancy states provide time windows to study stepwise deexcitation and the transfer of excitation energy to the reaction products. In particular, the satellite intensities and energy positions of the emitted x rays and Auger electrons provide important information on the history of the projectile ions interacting with the surface and the bulk material. In these types of studies the following physical processes and parameters are of major importance.

(a) The initial electronic configuration of the approaching ion and the surface potential of the solid determine the transfer of electrons from the surface into states with high-n quantum numbers.

(b) The approach velocity and the autoionization and radiative-decay rates determine the transfer of electrons to lower states or back to the solid, and together with (a) determine the distribution and time evolution of the population of different quantum states during neutralization.

(c) Transfer of electrons into a state with low quantum numbers occurs when the ion enters the surface.

A method to vary the ion-velocity component normal to surface, which has been used for $Ne^{9+,10+}$ and $Ar^{17+,18+}$ ion impact, is based on the change of the angle of ion impact between normal and grazing incidence. From an analysis of the corresponding K x-ray emission spectra (energy shifts and satellite-line intensities) the remaining number of inner-shell vacancies can be extracted. These results are generally very similar to those where the ions have been decelerated first to low velocity and then hit the surface at normal incidence. The ion-bulk interaction is more pronounced at higher approach velocities. In this case the inner-shell vacancies have a larger probability to penetrate the first surface layer and the interaction with the bulk may cause a fast filling of shells with lower-n quantum numbers with a simultaneous "peeling off" of electrons in shells with higher-n manifolds. States with intermediate-n quantum numbers can be filled either directly by electron transfer from the solid or by radiative or autoionizing decays. The balance between electron transfer and loss rates, autoionization and radiative transition rates, the approach velocity and the binding energies of the target and the projectile determine the specific population of n manifolds and the observed spectral-line intensities. We note that the innermost atomic shells are generally not filled by electron-capture reactions if the projectile velocity is too slow for direct electron transfer to occur. In this case surviving multiple inner-shell vacancy states can be used as an "inner atomic clock." This idea has been first applied by Briand *et al.* [3] studying satellite and hypersatellite K x-ray transitions in bare Ar ion-surface collisions.

In this paper we present data on the ion-surface neutralization dynamics using more highly charged Xe ions, characterized by an approach velocity of $v \approx 0.22$ a.u. corresponding to 7 Å/fs, where the number of L-shell vacancies in the incident Xe^{q+} ($q=44$ to 48) projectile is systematically changed. Here, $q=44+$ represents the closed shell $1s^2 2s^2 2p^6$ ground-state configuration of Xe and the other charge states are characterized by open L-shell configurations of the type $1s^2 2s^2 2p^5$ ($q=45+$), $1s^2 2s^2 2p^4$ ($q=46+$), $1s^2 2s^2 2p^3$ ($q=47+$), and $1s^2 2s^2 2p^2$ ($q=48+$) differing in the incident number of $2p$ holes.

As a first attempt to study experimentally the decay of highly excited Xe ions in the vicinity of a Cu surface, we have measured the L and M x-ray spectra as a function of the incident charge state. The experimental procedure is described in Sec. II. The description of the theoretical method used to predict radiative-transition energies and transition probabilities for Xe ions with different numbers of L-shell vacancies is presented in Sec. III. A more detailed description of our theoretical approach is given elsewhere [17]. A comparison of the predicted theoretical data with experimental results is presented in Sec. IV. Finally, the general trends of the experimental findings and important conclusions on the ion-surface and ion-bulk neutralization dynamics for the Xe^{q+}-plus-Cu system are discussed in Sec. V.

II. EXPERIMENT

In this paper we report measurements on ion-surface interactions for the impact of highly charged ions Xe^{q+} ($q=44-48$) on a solid surface. The Xe^{q+} ions have been extracted from the Lawrence Livermore EBIT source. In this work we only briefly address the operation of an EBIT and its upgrade to an ion source by means of an efficient extraction system which is described in detail in Ref. [2]. The EBIT basically consists of a three-segment axial drift-tube assembly. These segments may be individually biased to create an electrostatic well along the central axis. An electron beam, compressed to ≈ 70 μm in a 3-T magnetic field, travels along the central axis. The energy of the electrons is determined by the voltage applied to the drift-tube assembly. Typical electron-beam currents used range from 5 to 160 mA. Neutral gas atoms, such as Xe, are highly ionized by multiple electron impact and then trapped axially within the central well of the drift-tube potential and radially by the electron-beam space charge. After some confinement time they reach an equilibrium charge-state distribution due to successive ionization, excitation, recombination, and other ion-atom, ion-ion, and ion-electron interactions. After equilibrium is reached ($\tau \lesssim 1$ sec) the ions are ejected from the trap by applying an ejection voltage (e.g., 7 kV) to the drift-tube potentials and by raising the middle drift-tube potential. The ejected ions with energies given by the extraction voltage times the charge state q are then momentum analyzed and focused onto the target surface. In the present case the target surface was Cu which has been polished (≈ 10 μm roughness) but not chemically or sputter cleaned. The target is tilted by 45° with respect to the ion-beam axis and the x-ray emission

following electron capture and loss of the ions at the surface is observed with a Si(Li) detector perpendicular to the beam axis. The geometrical solid angle of this detector was 3×10^{-3} sr and its resolution about 170 eV at 5.9 keV, respectively. The detector was separated from the target chamber vacuum by Be foils (total thickness: 0.075 mm). For the Xe L x-ray line structures around 4.5 keV, photon absorption in the Be window is negligible. However, for the Xe M radiation at around 2 keV the observed line intensities are reduced by a factor of approximately 2 due to absorption.

The vacuum in the beam-transport system between the EBIT and the analyzing magnet was about 10^{-8} Torr and the charge change by electron capture from rest gas molecules was estimated to be small. Between the magnet and the Cu target a vacuum of the order of 10^{-8} Torr was maintained leading to an estimated loss of ions with inner-shell vacancies of less than 10%.

III. ENERGIES OF A MANY-ELECTRON SYSTEM

The calculation of theoretical x-ray spectra, including transition probabilities and autoionization rates for multiply excited Xe ions with up to 53 electrons represents a challenging many-body problem [17–29]. In this work we have performed comprehensive calculations of transition energies and transition probabilities associated with multiply excited states in Xe by using nonrelativistic and relativistic perturbation theory [24–28].

In particular, we have studied electric-dipole transitions of the type $2l$-$3l'$, $2l$-$4l'$, $2l$-$5l'$, $3l$-$4l'$, $3l$-$5l'$, and $4l$-$5l'$ for configurations

$$Q=1s_1^k2s_2^k2p_3^k3s_4^k3p_5^k3d_6^k4s_7^k4p_8^k4d_9^k4f_{10}^k5s_{11}^k5p_{12}^k \ , \quad (1)$$

with up to $N=53$ electrons occupying 12 different subshells, where k_i ($i=1$ to 12) are the electron occupation numbers. Our method allows the expression of the desired atomic properties in analytical form as a function of the electron numbers (k_i). As an important example we focus in this paper on x-ray energies and transition probabilities. The procedure to derive the nonrelativistic part of x-ray energies is outlined in the following.

A. Nonrelativistic part

In order to reduce the vast number of possible states, we have averaged over the spin and angular-momentum quantum numbers. These LS-averaged energy values can be expressed in first-order perturbation theory as [26]

$$E_1^N(Q)=\tfrac{1}{2}\sum_i k_i(k_i-1)U(n_il_i)+\sum_{i,j}k_ik_jU(n_il_i,n_jl_j) \ , \quad (2)$$

where the two-particle energies $U(nl), U(nl,n'l')$ are equal to

$$U(nl)=F_0(nl)\sum_{k(>0)}\frac{2l+1}{4l+1}\begin{bmatrix} l & l & k \\ 0 & 0 & 0 \end{bmatrix}^2 F_k(nl,nl) \ , \quad (3)$$

$$U(nl,n'l')=F_0(nl,n'l')-\tfrac{1}{2}\sum_k\begin{bmatrix} l & l' & k \\ 0 & 0 & 0 \end{bmatrix}^2 G_k(nl,n'l') \ , \quad (4)$$

and the radial integrals are determined in the usual way [24]

$$F_k(nl,n'l')=R_k(nln'l';n'l'nl) \ ,$$

$$G_k(nl,n'l')=R_k(nln'l';nln'l') \ ,$$

$$R_k(n_1l_1n_2l_2;n_4l_4n_3l_3)=\int_0^\infty r_1^2dr\int_0^\infty r_2^2dr\frac{r_<^k}{r_>^{k+1}}R_{n_2l_2}(r_2)\times R_{n_4l_4}(r_2)R_{n_3l_3}(r_1)R_{n_1l_1}(r_1) \ . \quad (5)$$

Substituting into (2) the numerical values for the radial integrals, we obtain for $E_1(Q)$

$$\begin{aligned}E_1^N(Q)=&\frac{k_1}{2}(k_1-1)0.625+\frac{k_2}{2}(k_2-1)0.150\,391+\frac{k_3}{2}(k_3-1)0.174\,609+\frac{k_4}{2}(k_4-1)0.066\,406\,2\\&+\frac{k_5}{2}(k_5-1)0.068\,988\,8+\frac{k_6}{2}(k_6-1)0.083\,663\,7+\frac{k_7}{2}(k_7-1)0.037\,271\,5\\&+\frac{k_8}{2}(k_8-1)0.037\,340\,9+\frac{k_9}{2}(k_9-1)0.041\,284\,9+\frac{k_{10}}{2}(k_{10}-1)0.049\,136\,5\\&+\frac{k_{11}}{2}(k_{11}-1)0.023\,830\,0+\frac{k_{12}}{2}(k_{12}-1)0.022\,808\,4+k_1k_20.198\,904+k_1k_30.234\,263\\&+k_1k_40.096\,603\,4+k_1k_50.106\,560+k_1k_60.11\,089\,9+k_1k_70.056\,463\,4+k_1k_80.060\,594\,2\\&+k_1k_90.062\,384\,2+k_1k_{10}0.062\,498\,3+k_1k_{11}0.036\,928+k_1k_{12}0.039\,027\,5\\&+k_2k_30.147\,461+k_2k_40.080\,375\,9+k_2k_50.088\,596\,6+k_2k_60.099\,925\,9\\&+k_2k_70.050\,154\,7+k_2k_80.053\,504\,0+k_2k_90.058\,018\,1+k_2k_{10}0.061\,837\,2+k_2k_{11}0.033\,794\\&+k_2k_{12}0.035\,493\,0+k_3k_40.085\,185\,4+k_3k_50.091\,598\,5+k_3k_60.102\,905+k_3k_70.051\,861\,1\\&+k_3k_80.054\,723\,6+k_3k_90.059\,149\,7+k_3k_{10}0.062\,100\,9+k_3k_{11}0.034\,613\,5+k_3k_{12}0.036\,11\\&+k_4k_50.061\,740\,7+k_4k_60.070\,855\,1+k_4k_70.043\,015\,2+k_4k_80.045\,800+k_4k_90.049\,052\end{aligned}$$

$$+k_4k_{10}0.054\,434\,6+k_4k_{11}0.030\,527\,5+k_4k_{12}0.031\,830\,6+k_5k_6 0.073\,622+k_5k_7 0.044\,866\,5$$
$$+k_5k_8 0.046\,401\,3+k_5k_9 0.050\,208\,3+k_5k_{10}0.055\,501\,1+k_5k_{11}0.031\,256\,6+k_5k_{12}0.032\,160\,4$$
$$+k_6k_7 0.046\,749\,1+k_6k_8 0.048\,611+k_6k_9 0.052\,399\,5+k_6k_{10}0.058\,522\,7+k_6k_{11}0.032\,104\,5$$
$$+k_6k_{12}0.033\,131\,6+k_7k_8 0.029\,884\,4+k_7k_9 0.037\,926\,7+k_7k_{10}0.040\,885+k_7k_{11}0.026\,676$$
$$+k_7k_{12}0.027\,965\,5+k_8k_9 0.038\,413\,1+k_8k_{10}0.041\,51+k_8k_{11}0.027\,622\,4+k_8k_{12}0.028\,140\,4$$
$$+k_9k_{10}0.044\,109\,2+k_9k_{11}0.028\,450\,8+k_9k_{12}0.029\,085\,6+k_{10}k_{11}0.029\,427\,4$$
$$+k_{10}k_{12}0.030\,139\,4+k_{11}k_{12}0.021\,504\,5\ . \tag{6}$$

In zero approximation a simple expression has been derived for the energy of each Q state,

$$E_0^N(Q)=-\tfrac{1}{2}\left[k_1+\frac{k_2+k_3}{4}+\frac{k_4+k_5+k_6}{9}+\frac{k_7+k_8+k_9+k_{10}}{16}+\frac{k_{11}+k_{12}}{25}\right]. \tag{7}$$

$E_0^N(Q)$ and $E_1^N(Q)$ are generally not very good approximations for any atomic system; however, the accuracy of the method can be improved by using the following screening approach:

$$E^N(Q)=E_0^N(Q)\left[Z+\frac{E_1^N(Q)}{2E_0^N(Q)}\right]^2, \tag{8}$$

which incorporates part of the second-order approximation.

It was shown [27] that almost 90% of E_2^N was actually taken into account by using the above formula. The same type of screening procedure can be applied for the calculation of $n_1l_1-n_2l_2$ x-ray transition energies, namely,

$$\begin{aligned}E^N(Q)-E^N([n_1l_1]^{-1}n_2l_2Q)&\cong Z^2[E_0^N(n_1l_1)-E_0^N(n_2l_2)]\\&\quad+Z\{E_1^N(Q)-E_1^N([n_1l_1]^{-1}n_2l_2Q)\}\\&=[E_0^N(n_1l_1)-E_0^N(n_2l_2)](Z-\sigma^N)^2\ ,\\ \sigma^N&=\frac{-\{E_1^N(Q)-E_1^N([n_1l_1]^{-1}n_2l_2Q)\}}{2[E_0^N(n_1l_1)-E_0^N(n_2l_2)]}\ ,\\ E^N(nl)&=-1/2n^2\ .\end{aligned} \tag{9}$$

In the calculations performed in this work, n_1l_1, n_2l_2 are fixed and the occupation numbers k_i of electrons in each subshell varied. Specifically, we have adopted the following notation for each initial inner-hole state, namely:

$$[n_1l_1]^{-1}n_2l_2Q\ , \tag{10}$$

where $[n_1l_1]^{-1}$ characterizes the inner-shell vacancy to be filled, n_2l_2 the active electron involved in the electric-dipole transition, and Q represents the additional spectator electrons distributed over various subshells.

B. Relativistic corrections

For intermediate-Z atoms, like Xe, relativistic effects may be accounted for by adding additional terms to the nonrelativistic Hamiltonian resulting from the reduction of the Dirac equation and the Breit interaction [29]. Since we are interested in LS-averaged energies, only those terms of the Breit operator which cause energy shifts are incorporated here. These operators can be written as [24]

$$\begin{aligned}H_1(\mathbf{r})&=-\frac{\alpha^2}{2}\mathbf{p}^4\ ,\\ H_{4'}(\mathbf{r})&=\frac{\alpha^2}{2}\pi Z\delta(\mathbf{r})\ ,\\ H_{4''}(\mathbf{r}_{12})&=-\alpha^2\pi\delta(\mathbf{r}_{12})\ ,\\ H_2(\mathbf{r}_{12})&=-\frac{\alpha^2}{2}\frac{1}{r_{12}}\left[\mathbf{p}_1\cdot\mathbf{p}_2+\frac{\mathbf{r}_{12}(\mathbf{r}_{12}\cdot\mathbf{p}_1)\cdot\mathbf{p}_2}{\mathbf{r}_{12}^2}\right],\\ H_{5''}(\mathbf{r}_{12})&=-\frac{8}{3}\alpha^2\pi\mathbf{s}_1\cdot\mathbf{s}_2\delta(\mathbf{r}_{12})\ .\end{aligned} \tag{11}$$

The matrix elements for two one-particle operators H_1 and $H_{4'}$ are equal in zero approximation for all Q states, therefore

$$\langle Q|H_1+H_{4'}|Q\rangle^{(0)}=-\alpha^2Z^4\sum_i q(n_il_i)E_0^R(n_il_i)\ , \tag{12}$$

where

$$E_0^R(nl)=-\frac{2}{n^3}\left[\frac{2}{2l+1}-\frac{3}{4n}-\delta(1,0)\right]. \tag{13}$$

In our case the numerical evaluation of Eq. (12) yields

$$\begin{aligned}&\langle Q|H_1+H_{4'}|Q\rangle^{(0)}\\&=-\alpha^2Z^4\left[\tfrac{1}{8}k_1+\tfrac{5}{128}k_2+\tfrac{7}{384}k_3+\tfrac{1}{72}k_4+\tfrac{5}{648}k_5+\tfrac{1}{360}k_6+\frac{13}{2^{11}}k_7+\frac{23}{3\times2^{11}}k_8+\frac{17}{5\times2^{11}}k_9+\frac{11}{7\times2^{11}}k_{10}+\tfrac{27}{5000}k_{11}+\tfrac{31}{15\,000}k_{12}\right].\end{aligned} \tag{14}$$

We further note that the zero-order approximation for the three-particle operators H_2, $H_{5''}$, and $H_{4''}$ are proportional to Z^3. Thus

$$\langle Q|H_2+H_{4''}+H_{5''}|Q\rangle^{(0)}\cong\alpha^2Z^3F(Q)\ . \tag{15}$$

The calculation of $F(Q)$ is described in detail in [24]. It is sufficient to calculate only the two radial integrals, T and K,

$$T(n_1l_1n_2l_2;n_4l_4n_3l_3)=\int_0^\infty r_1^2dr\, R_{n_1l_1}(r_1)R_{n_2l_2}(r_2)R_{n_4l_4}(r_2)R_{n_3l_3}(r_1)\ , \tag{16}$$

$$K_l(n_1l_1n_2l_2;n_4l_4n_3l_3)=\int_0^\infty r_1^2dr_1\int_0^\infty r_2^2dr_2\theta(r_1-r_2)\frac{r_2^l}{r_1^{l+1}}R_{n_1l_1}(r_1)R_{n_2l_2}(r_2)\frac{d^2}{dr_1dr_2}R_{n_4l_4}(r_2)R_{n_3l_3}(r_1)\ . \tag{17}$$

Moreover, the angular part for the two-particle operators $H_2+H_{4''}+H_{5''}$ is the same as for the $1/r_{12}$ electrostatic operator. Hence, Eqs. (2)–(5) can be applied to evaluate the corresponding relativistic matrix elements. The same equations have also been used to determine the first-order corrections originating from the one-particle operators H_1 and $H_{4'}$. The radial part of the relativistic first-order contribution is [24]

$$E_k^i(n_1l_1n_2l_2;n_4l_4n_3l_3)=\sum_n\frac{1}{E_n+E_{n_2}-E_{n_4}-E_{n_3}}\begin{bmatrix}l & l_1 & l_3\\ 0 & 0 & 0\end{bmatrix}\begin{bmatrix}l & l_2 & l_4\\ 0 & 0 & 0\end{bmatrix}M^i(nl,n_1l_1)R_k(n_1l_1n_2l_2;n_4l_4n_3l_3)\ , \tag{18}$$

with

$$M^i(nl,n'l')=-\tfrac{1}{2}\delta(l,l')\int_0^\infty r^2dr\left[\frac{2}{r}-\frac{1}{n^2}\right]\left[\frac{2}{r}-\frac{1}{(n')^2}\right]R_{nl}(r)R_{n'l'}(r)\ , \tag{19}$$

$$M^{4'}(nl,n'l')=-\tfrac{1}{2}\delta(l,0)\delta(l',0)R_{nl}(0)R_{n'l'}(0)\ . \tag{20}$$

Summation in (15) extends over the discrete part of the spectrum and includes integration over the continuous part [24]. In this study we have calculated all the relevant expressions, i.e., T, K_1, E_k^1, and $E_k^{4'}$ for all possible nl values associated with different Q states. In particular, we have found that all terms scale as Z^3 and hence

$$\langle Q|H_2+H_{4''}+H_{5''}|Q\rangle^{(0)}+\langle Q|H_1+H_{4'}|Q\rangle^{(1)}=\alpha^2Z^3E_1^R(Q)\ . \tag{21}$$

Here we have evaluated $E_1^R(Q)$ for the inner $1s$, $2s$, $2p$, $3s$, $3p$, and $3d$ shells

$$\begin{aligned}
&E_1^R(1s^{k_1}2s^{k_2}2p^{k_3}3s^{k_4}3p^{k_5}3d^{k_6})\\
&=\frac{k_1}{2}(k_1-1)0.480\,140+\frac{k_2}{2}(k_2-1)0.060\,886\,5+\frac{k_3}{2}(k_3-1)0.044\,092\,5+\frac{k_4}{2}(k_4-1)0.019\,005\,6\\
&\quad+\frac{k_5}{2}(k_5-1)0.012\,891\,0+\frac{k_6}{2}(k_6-1)0.007\,579\,75+\frac{k_7}{2}(k_7-1)0.008\,02+\frac{k_8}{2}(k_8-1)0.005\,44\\
&\quad+\frac{k_9}{2}(k_9-1)0.003\,20+\frac{k_{10}}{2}(k_{10}-1)0.002\,50+\frac{k_{11}}{2}(k_{11}-1)0.004\,11+\frac{k_{12}}{2}(k_{12}-1)0.002\,78\\
&\quad+k_1k_20.100\,071+k_1k_30.081\,704\,8+k_1k_40.039\,433+k_1k_50.032\,103\,2+k_1k_60.011\,363\\
&\quad+k_1k_70.018\,886+k_1k_80.015\,372+k_1k_90.006\,766+k_1k_{10}0.003\,073+k_1k_{11}0.010\,278\\
&\quad+k_1k_{12}0.008\,345+k_2k_30.049\,104+k_2k_40.025\,026\,1+k_2k_50.022\,652+k_2k_60.015\,815\\
&\quad+k_2k_70.033\,55+k_2k_80.011\,327+k_2k_90.007\,649+k_2k_{10}0.003\,737+k_2k_{11}0.007\,570\\
&\quad+k_2k_{12}0.006\,378+k_3k_40.025\,932+k_3k_50.019\,465+k_3k_60.012\,703+k_3k_70.013\,422\\
&\quad+k_3k_80.010\,158+k_3k_90.006\,786+k_3k_{10}0.003\,270+k_3k_{11}0.007\,608+k_3k_{12}0.005\,763\\
&\quad+k_4k_50.012\,86+k_4k_60.005\,31+k_4k_70.013\,31+k_4k_80.008\,23+k_4k_90.003\,91\\
&\quad+k_1k_{10}0.003\,737+k_4k_{11}0.007\,570+k_4k_{12}0.004\,93+k_5k_60.005\,52+k_5k_70.013\,67\\
&\quad+k_5k_80.008\,34+k_5k_90.004\,00+k_5k_{10}0.002\,03+k_5k_{11}0.007\,97+k_5k_{12}0.004\,98\\
&\quad+k_6k_70.014\,24+k_6k_80.008\,73+k_6k_90.004\,18+k_6k_{10}0.002\,16+k_6k_{11}0.008\,19\\
&\quad+k_6k_{12}0.005\,14+k_7k_80.005\,37+k_7k_90.003\,02+k_7k_{10}0.001\,51+k_7k_{11}0.006\,80\\
&\quad+k_7k_{12}0.004\,33+k_8k_90.003\,06+k_8k_{10}0.001\,53+k_8k_{11}0.007\,04+k_8k_{12}0.004\,36\\
&\quad+k_9k_{10}0.001\,62+k_9k_{11}0.007\,25+k_9k_{12}0.004\,51+k_{10}k_{11}0.007\,50+k_{10}k_{12}0.004\,67+k_{11}k_{12}0.004\,56\ .
\end{aligned} \tag{22}$$

TABLE I. Range of $3d$-$2p$ transitions for Xe ions with $2p$ vacancies.

Number of $2p$ holes	X-ray energies (eV)	Approximate width of structure (eV)	Energy shift (eV)	Radiative transition probabilities (10^{13} s^{-1})
1	4053–4647	594	102	5.4–51.0
2	4147–4749	602	102	11.7–109.0
3	4243–4851	608	102	18.7–137.9
4	4339–4955	616	104	26.6–248.6
5	4437–5060	623	105	35.4–331.3
6	4536–5166	630	106	45.2–423.7

The zero- (E_0^R) and first- (E_1^R) order energies can be represented in the form of a screening formula similar to Eq. (8) for $E^N(Q)$,

$$E^R(Q)=\alpha^2 Z E_0^R(Q)\left[Z+\frac{E_1^R(Q)}{3E_0^R(Q)}\right]^3 . \tag{23}$$

Then the resulting total energy $E(Q)$ can be expressed as

$$E(Q)=E^N(Q)+E^R(Q) , \tag{24}$$

where $E^N(Q)$ and $E^R(Q)$ are the nonrelativistic and relativistic contributions, respectively. Finally the x-ray transition energies may be written as

$$\begin{aligned} E(Q)-E([n_1l_1]^{-1}n_2l_2Q) &= [E^N(n_1l_1)-E_0^N(n_2l_2)](Z-\sigma^N)^2 \\ &\quad +\alpha^2 Z[E_0^R(n_1l_1)-E_0^R(n_2l_2)](Z-\sigma^R)^3 , \end{aligned} \tag{25}$$

where σ^N and σ^R are equal to

$$\begin{aligned} \sigma^N &= -\frac{\{E_1^N(Q)-E_1^N([n_1l_1]^{-1}n_2l_2Q)\}}{2[E_0^N(n_1ln_1)-E_0^N(n_2l_2)]} , \\ \sigma^R &= -\frac{\{E_1^R(Q)-E_1^R([n_1l_1]^{-1}n_2l_2Q)\}}{3[E_0^R(n_1l_1)-E_0^R(n_2l_2)]} . \end{aligned} \tag{26}$$

As a representative example the relevant $2p$-$3d$ x-ray energies (Q-$2p^{-1}3dQ$) are discussed in more detail.

For each L spectrum correlated with a specific $2p$-hole state, i.e.,

$$\begin{aligned} &\Phi_0\Phi_1-2p^{-1}3d\Phi_0\Phi_1 , \\ &\Phi_0=1s^2 2s^2 2p^6 , \\ &\Phi_1=3s^{k_4}3p^{k_5}3d^{k_6}4s^{k_7}4p^{k_8}4d^{k_9}5s^{k_{11}}5p^{k_{12}} . \end{aligned} \tag{27}$$

The key parameters in our theoretical model of multiply core-excited states are the occupation numbers k_i, in particular, the number of $2p$ and $3d$ electrons are of primary importance. Table I clearly indicates that changing the number of $2p$ vacancies by one shifts the L x-ray energies by about 102–106 eV. On the other hand, adding one extra $3d$ electron decreases the energy by about 26 eV. To obtain accurate L and M x-ray energies, relativistic corrections have been included in the calculation. As an illustrative example we present here relativistic corrections for $3d$-$2p$ transitions characterized by $1s^2 2s^2 2p^k - 1s^2 2s^2 2p^{k-1}$ with varying initial $2p^k$ hole states, where k is ranging from $k=1$ to 6. As can be seen relativistic corrections for the $3d$-$2p$ decay are of the order 119–141 eV, depending on the specific $2p^k$ core states (see Table II). These results agree within a few eV with recent multiconfiguration Dirac-Fock calculations.

C. Transition probabilities

In this study we have also investigated transition probabilities within the framework of the LS-averaged approximation. As an example we present here the analytic formula for LS-averaged transition probabilities

$$W(Q,[n_1l_1]^{-1}n_2l_2Q)=A_0(n_1l_1,n_2l_2)Z^4\frac{k_1}{g_1}\left[1-\frac{k_2}{g_2}\right]\left[\frac{E(Q)-E([n_1l_1]^{-1}n_2l_2Q)}{E_0(Q)-E_0([n_1l_1]^{-1}n_2l_2Q)}\right]^3\left[1-\frac{P(k_1)}{Z}\right]^2 , \tag{28}$$

where $g_i=2(2l_i+1)$ are the statistical weights and $P(k_i)$ the first-order correction for dipole matrix elements. The hydrogenic transition probabilities $A_0(10^8$ s$^{-1})$ are listed in Table III. It is evident from this table that the $3d$-$2p$, $4d$-$2p$, $4f$-$3d$, and $5g$-$4f$ transitions are characterized by large transition probabilities. For the L spectra we expect the $2p$-$3d$ decays to dominate the observed x-ray 350 different $2p$-$3d$ transition energies have been calculated [17,23]. Due to the limited resolution of our x-ray detector, these lines have been treated as a quasicontinuum with an energy-band width of roughly 600 eV. $2p$-$3d$ transitions with ten electrons have the largest energy values while those transitions with the maximum number of electrons ($N \leq 53$) are shifted to lower energies by about 600 eV. The energy range of $3d$-$2p$ transitions for different $2p$ hole configurations in Xe are summarized in Table I.

TABLE II. Relativistic corrections for $3d$-$2p$ transitions characterized by $1s^2 2s^2 2p^{k-1}3d - 1s^2 2s^2 2p^k$ initial-to-final-state configurations.

k	1	2	3	4	5	6
E^R (eV)	149	141	135	130	124	119

TABLE III. Averaged hydrogenic transition probabilities $A_0(nl,n'l')$ in units of 10^8 s^{-1}.

nl-$n'l'$	A_0	nl-$n'l'$	A_0	nl-$n'l'$	A_0	nl-$n'l'$	A_0
$2p$-$1s$	37.575	$3s$-$2p$	0.1262	$3d$-$2p$	6.4625	$4p$-$3d$	0.020 84
$3p$-$1s$	10.106	$4s$-$2p$	0.051 54	$4d$-$2p$	2.0617	$5p$-$3d$	0.008 97
$4p$-$1s$	4.0896	$5s$-$2p$	0.025 76	$5d$-$2p$	0.9422	$6p$-$3d$	0.004 69
$5p$-$1s$	2.0617	$6s$-$2p$	0.014 02	$6d$-$2p$	0.4906	$5p$-$4d$	0.011 30
$6p$-$1s$	1.1706	$4s$-$3p$	0.036 69	$4d$-$3p$	0.7035	$6p$-$4d$	0.005 65
$3p$-$2s$	1.3464	$5s$-$3p$	0.018 09	$5d$-$3p$	0.3390	$4f$-$3d$	1.9296
$4p$-$2s$	0.5799	$6s$-$3p$	0.010 14	$6d$-$3p$	0.1877	$5f$-$3d$	0.6356
$5p$-$2s$	0.2968	$5s$-$4p$	0.012 90	$5d$-$4p$	0.1485	$6f$-$3d$	0.3003
$6p$-$2s$	0.1635	$6s$-$4p$	0.007 162	$6d$-$4p$	0.086 18	$5f$-$4d$	0.3617
$4p$-$3s$	0.1838			$5d$-$4f$	0.050 46	$6f$-$4d$	0.1801
$5p$-$3s$	0.077 70			$6d$-$4f$	0.021 44	$5g$-$4f$	0.7654
$6p$-$3s$	0.057 28					$6g$-$4f$	0.2470
$5p$-$4s$	0.044 21						
$6p$-$4s$	0.026 73						

features. Furthermore, from Table III it may be inferred that $3d$-$4f$ transitions are of major significance for the observed M x-ray spectra. The experimental results are discussed in the following section.

IV. RESULTS AND DISCUSSION

Figure 1 gives an overview of the observed x-ray spectra originating from Xe^{44+} to Xe^{48+} ions impinging on Cu surfaces. As can be seen the Xe^{44+} spectrum [Fig. 1(a)] consists only of lower-energy M x-ray peaks due to the missing L vacancy states of the incoming projectile ion. From this figure we can also deduce that no additional L-shell vacancies are produced during the impact of the ion on the surface. In contrast the spectra resulting from Xe^{45+} to Xe^{48+} initial projectiles show, as expected, higher-energy L x-ray-line structures, which arise predominantly from electric-dipole transitions into empty $2p$ states. In accordance with the increasing number of $2p$ vacancies (see Table I and the Appendix), the measured L line energy positions shift towards higher energies with increased charge state q. Due to many satellite-line groups and limited energy resolution of our Si (Li) detector the observed line intensities are averaged over several closely spaced line groups. For the following discussion we have displayed the Xe^{44+}, Xe^{45+}, and Xe^{48+} spectra in more detail in Figs. 2(a)–2(c). For a comparison we have indicated the range of the calculated $2p$-$3d$ transition energies in Figs. 2(b) and 2(c) for the satellite groups originating from $1s^2 2s^2 2p^k$ ($k=2-5$) initial inner-hole-state configurations. These include about 350 possible satellite groups (see the Appendix) with centroid energies varying from 4053 to 5166 eV for Xe^{45+} and 4×350 satellite groups for Xe^{48+} projectiles with a total-energy variation of about 4053 to 4955 eV. The simplest case is Xe^{45+}, where the projectile ion arrives at the surface with only one $2p$ hole. The following configurations of multiply excited states with main quantum numbers $n \leq 4$ and angular-momentum states $l \leq 2$ were con-

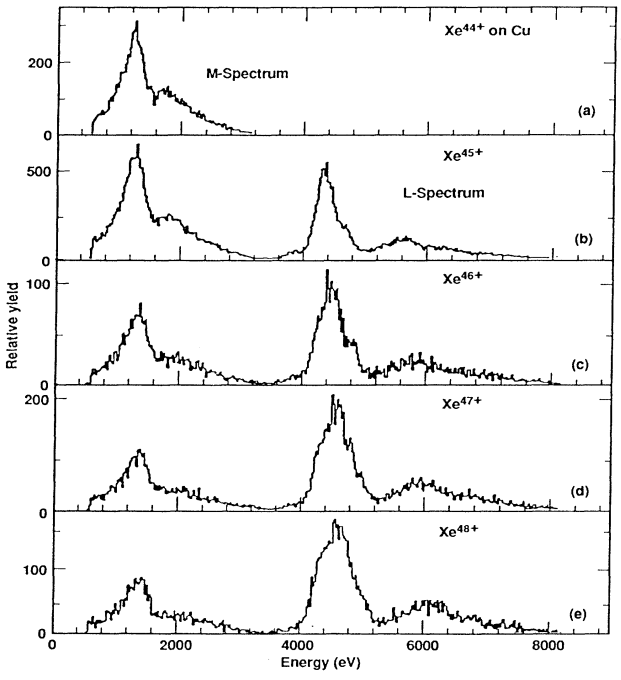

FIG. 1. (a)–(e) Xe M,L x-ray spectra following $7q$ keV Xe^{q+} ($q=44-48$) ion impact on a Cu surface as a function of the projectile charge q.

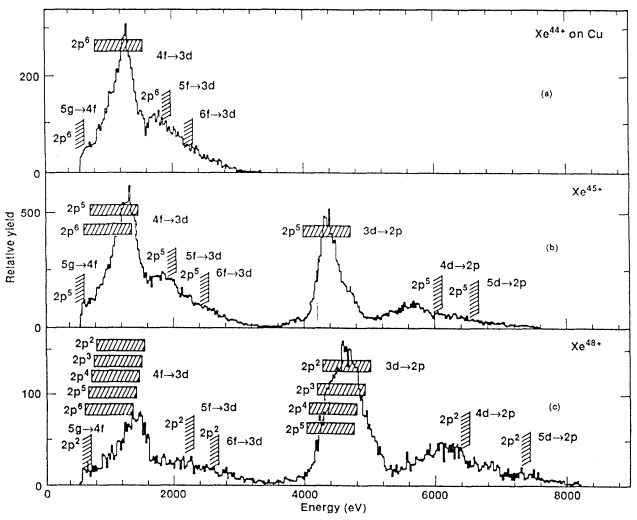

FIG. 2. Comparison of observed and predicted x-ray structures for (a) Xe^{44+}, (b) Xe^{45+}, and (c) Xe^{48+}.

sidered to contribute to the main intensity of the observed $2p$-$3d$ transitions [see Fig. 2(b) and the Appendix],

$1s^2 2s^2 2p^5 3s^2 3p^6 3d\ 4s^2 4p^6 4d^6$,

$1s^2 2s^2 2p^5 3s^2 3p^6 3d\ 4s^2 4p^6 4d^3$,

$1s^2 2s^2 2p^5 3s^2 3p^6 3d^2\ 4s^2 4p^6$,

$1s^2 2s^2 2p^5 3s^2 3p^6 3d^4\ 4s^2 4p^3$,

$1s^2 2s^2 2p^5 3s^2 3p^6 3d^5\ 4s^2$,

$1s^2 2s^2 2p^5 3s^2 3p^5 3d^6$,

$1s^2 2s^2 2p^5 3s^2 3p^4 3d^7$,

$1s^2 2s^2 2p^5 3s^2 3p^3 3d^8$,

$1s^2 2s^2 2p^5 3s^2 3p^2 3d^9$,

$1s^2 2s^2 2p^5 3s^2 3p\ 3d^{10}$.

Even though the maximum of the measured structures

TABLE IV. Transition energies E (eV) for ions with $Z=54$ (Xe^{44+}) $\Phi_0\Phi_1-2p^{-1}3d\Phi_0\Phi_1$; $\Phi_0=1s^2 2s^2 2p^6$; $\Phi_1=3s^{n4}3p^{n5}3d^{n6}4s^{n7}4p^{n8}4d^{n9}5s^{n11}5p^{12}$; $N=10+n_4+n_5+n_6+n_7+n_8+n_9+n_{11}+n_{12}$; $n_4=1$–2, $n_5=0$–6, $n_7=0$–2, $n_8=0$–8, $n_9=0$–10, $n_{11}=0$–2, $n_{12}=0$–6. I, $\Phi_1=3d^n\Phi_0$, $n=0$–9, where $N=n_4+n_5+n_7+n_8+n_{11}+n_{12}$; II, $\Phi_1=\Phi_0 3s^{n4}3p^{n5}4s^{n7}4p^{n8}4d^{n9}5s^{n11}5p^{n12}=\Phi^*$; III, $\Phi_1=3d\Phi^*$; IV, $\Phi_1=3d^2\Phi^*$; V, $\Phi_1=3d^3\Phi^*$; VI, $\Phi_1=3d^4\Phi^*$; VII, $\Phi_1=3d^5\Phi^*$; VIII, $\Phi_1=3d^6\Phi^*$; IX, $\Phi_1=3d^7\Phi^*$; X, $\Phi_1=3d^8\Phi^*$; XI, $\Phi_1=3d^9\Phi^*$.

N	I	II	III	IV	V	VI	VII	VIII	IX	X	XI
10	4647										
11	4621	4626									
12	4595	4606	4600								
13	4568	4580	4579	4574							
14	4542	4555	4554	4553	4548						
15	4516	4530	4529	4528	4527	4521					
16	4490	4505	4504	4503	4502	4501	4495				
17	4464	4480	4479	4478	4477	4476	4475	4469			
18	4438	4455	4454	4453	4452	4451	4450	4449	4443		
19	4412	4449	4429	4428	4427	4426	4425	4424	4423	4418	
20		4442	4423	4484	4403	4401	4400	4399	4398	4397	4392
21		4434	4416	4397	4378	4377	4376	4375	4374	4373	4371
22		4426	4408	4390	4371	4352	4351	4350	4349	4348	4347
23		4418	4400	4382	4365	4346	4327	4326	4325	4323	4322
24		4410	4392	4375	4357	4339	4320	4301	4300	4299	4298
25		4402	4384	4367	4349	4331	4314	4295	4276	4275	4274
26		4394	4377	4359	4341	4323	4306	4288	4269	4250	4249
27		4386	4369	4351	4333	4315	4298	4280	4263	4244	4225
28		4377	4360	4343	4325	4308	4290	4272	4255	4237	4219
29		4368	4351	4334	4317	4300	4282	4265	4247	4230	4212
30		4359	4342	4326	4309	4292	4274	4257	4239	4222	4204
31		4351	4334	4317	4300	4283	4267	4249	4232	4214	4197
32		4342	4325	4308	4291	4275	4258	4241	4224	4206	4189
33		4333	4316	4300	4283	4266	4249	4233	4216	4199	4181
34		4325	4308	4291	4274	4257	4241	4224	4207	4191	4174
35		4316	4299	4282	4266	4249	4232	4216	4199	4182	4166
36		4307	4291	4274	4257	4240	4224	4207	4190	4174	4157
37		4304	4282	4265	4248	4232	4215	4198	4182	4165	4149
38		4301	4279	4257	4240	4223	4206	4190	4173	4157	4140
39		4297	4275	4253	4231	4215	4198	4181	4165	4148	4132
40		4293	4272	4250	4228	4206	4189	4173	4156	4140	4123
41		4289	4268	4246	4225	4203	4181	4164	4148	4131	4115
42		4286	4264	4243	4221	4200	4178	4156	4139	4123	4106
43		4282	4260	4239	4217	4196	4175	4153	4131	4114	4098
44		4278	4256	4235	4214	4192	4171	4149	4128	4106	4090
45			4253	4231	4210	4188	4167	4146	4125	4103	4081
46				4227	4206	4185	4163	4142	4121	4100	4078
47					4202	4181	4159	4138	4117	4096	4075
48						4177	4156	4134	4113	4092	4071
49							4152	4131	4110	4088	4067
50								4127	4106	4085	4064
51									4102	4081	4060
52										4077	4056
53											4053

lies in the energy range predicted for the satellite group listed above, there is a tail of the intensity to higher energy with a shoulder at about 4.7 keV. Additionally one observes a group of lines at around 5.6–6 keV which originates mainly from $4d$-$2p$ transitions. A striking feature is the substantial shift of the position of the maximum in the L intensity from Xe^{45+} to Xe^{48+} of about 300 eV in accordance with the predicted shift of about 308 eV (see Table I).

By comparing the line profile of the $3d$-$2p$ structure for Xe^{48+} with the Xe^{45+} profile, we find that the L-line structure of the Xe^{48+} spectrum is much broader than the corresponding Xe^{45+} peak due to the subsequent filling of the L shell. The fact that the intensity originating from the $1s^2 2s^2 2p^2$ core state is higher than for $1s^2 2s^2 2p^5$ could have the following reasons: The lower energetic L x rays associated with the $2p^3$, $2p^4$, and $2p^5$ core states may be emitted by sequential filling at a later state of the ion-surface interaction in combination with cascade feeding, for example from $5g$-$4f$-$3d$ decays, when the ions have already penetrated into the solid.

In Figs. 2(b) and 2(c) we have also indicated the series

TABLE V. Transition energies (eV) for ions with $Z=54$ (Xe^{45+}) $\Phi_0\Phi_1-2p^{-1}3d\Phi_0\Phi_1$; $\Phi_0=1s^2 2s^2 2p^5$; $\Phi_1=3s^{n4}3p^{n5}3d^{n6}4s^{n7}4p^{n8}4d^{n9}5s^{n11}5p^{n12}$; $N=9+n_4+n_5+n_6+n_7+n_8+n_9+n_{11}+n_{12}$; $n_4=1-2$, $n_5=0-6$, $n_7=0-2$, $n_8=0-8$, $n_9=0-10$, $n_{11}=0-2$, $n_{12}=0-6$. I, $\Phi_1=3d^n\Phi_0$, $n=0-9$; II, $\Phi_1=\Phi_0 3s^{n4}3p^{n5}4s^{n7}4p^{n8}4d^{n9}5s^{n11}5p^{n12}=\Phi^*$; III, $\Phi_1=3d\Phi^*$; IV, $\Phi_1=3d^2\Phi^*$; V, $\Phi_1=3d^3\Phi^*$; VI, $\Phi_1=3d^4\Phi^*$; VII, $\Phi_1=3d^5\Phi^*$; VIII, $\Phi_1=3d^6\Phi^*$; IX, $\Phi_1=3d^7\Phi^*$; X, $\Phi_1=3d^8\Phi^*$; XI, $\Phi_1=3d^9\Phi^*$.

N	I	II	III	IV	V	VI	VII	VIII	IX	X	XI
9	4749										
10	4722	4728									
11	4695	4706	4701								
12	4669	4681	4680	4674							
13	4642	4655	4654	4653	4648						
14	4616	4630	4629	4628	4627	4621					
15	4589	4605	4604	4603	4601	4600	4595				
16	4563	4580	4578	4577	4576	4575	4574	4569			
17	4537	4554	4553	4552	4551	4550	4549	4548	4542		
18	4511	4548	4528	4527	4526	4525	4524	4523	4516		
19		4541	4521	4502	4501	4500	4499	4498	4497	4496	4490
20		4533	4515	4495	4476	4475	4474	4473	4472	4471	4470
21		4525	4507	4489	4469	4450	4449	4448	4447	4446	4445
22		4517	4499	4481	4463	4443	4424	4423	4422	4421	4420
23		4509	4491	4473	4455	4437	4418	4398	4397	4396	4395
24		4501	4483	4465	4447	4429	4411	4392	4373	4372	4371
25		4493	4475	4457	4439	4421	4403	4385	4366	4347	4346
26		4484	4467	4449	4431	4413	4395	4377	4360	4341	4322
27		4475	4458	4441	4423	4405	4387	4369	4352	4334	4315
28		4466	4449	4432	4415	4397	4379	4362	4344	4326	4308
29		4457	4440	4423	4406	4389	4371	4354	4336	4318	4301
30		4449	4432	4414	4397	4380	4363	4346	4328	4310	4293
31		4440	4423	4406	4389	4372	4355	4338	4320	4303	4285
32		4431	4414	4397	4380	4363	4346	4329	4312	4295	4277
33		4422	4405	4388	4371	4354	4337	4321	4304	4287	4269
34		4414	4396	4379	4363	4346	4239	4312	4295	4278	4262
35		4405	4388	4371	4354	4337	4320	4303	4286	4270	4253
36		4401	4379	4362	4345	4328	4321	4295	4278	4261	4244
37		4398	4376	4353	4336	4320	4303	4286	4269	4252	4236
38		4394	4373	4350	4328	4311	4294	4277	4261	4244	4227
39		4391	4369	4347	4325	4302	4285	4269	4252	4235	4219
40		4387	4365	4343	4321	4299	4277	4260	4243	4227	4210
41		4383	4361	4339	4317	4296	4274	4251	4235	4218	4201
42		4379	4357	4335	4314	4292	4270	4248	4226	4210	4193
43		4375	4353	4332	4310	4288	4267	4245	4223	4201	4184
44			4349	4328	4306	4284	4263	4241	4220	4198	4176
45				4324	4302	4281	4259	4238	4216	4195	4173
46					4298	4277	4255	4234	4212	4191	4170
47						4273	4251	4230	4208	4187	4166
48							4248	4226	4205	4183	4162
49								4222	4201	4180	4158
50									4197	4176	4155
51										4172	4151
52											4147

limits of $4d$-$2p$ transitions for the different possible core configurations. It is evident from this figure that the main intensity of the high-energy peaks in the L-line group stems from transitions associated with $4d$ states. One can even see some intensity from $5d$ and $6d$ states. In addition, we have studied the M x-ray spectra exhibited in Figs. 1(a)–1(e) and Figs. 2(a)–2(c), respectively. In fact, the most significant radiative transitions observed may arise from $4f$ states, which are most probably populated by direct capture into $n=4$ which in turn may lead to a strong excitation of $n=3$ levels via cascade mechanisms [30] when the ions have already penetrated into the solid. Considering the lower detection efficiency for the M x rays ($\sim$ factor of 2) compared to the L x rays it is obvious that the M intensities are actually larger than the L intensities. From the comparison of the observed line energies and our theoretical calculations we have found that the main peak in the M x-ray group arise from a population of $n=4$ states. Moreover, the peak on the high-energy side of the $n=4$ structure is due to $n\geq 5$ states. By comparing the maxima for the 4-3 ($n=4$ to $n=3$) transition for Xe^{45+} and Xe^{48+} [see Figs. 2(b) and

TABLE VI. Transition energies (eV) for ions with $Z=54$ (Xe^{46+}) $\Phi_0\Phi_1-2p^{-1}3d\Phi_0\Phi_1$; $\phi_0=1s^2 2s^2 2p^4$; $\Phi_1=3s^{n4}3p^{n5}3d^{n6}4s^{n7}4p^{n8}4d^{n9}5s^{n11}5p^{n12}$; $N=8+n_4+n_5+n_6+n_7+n_8+n_9+n_{11}+n_{12}$; $n_4=1$–2, $n_5=0$–6, $n_7=0$–2, $n_8=0$–8, $n_9=0$–10, $n_{11}=0$–2, $n_{12}=0$–6. I, $\Phi_1=3d^n\Phi_0$, $n=0$–9; II, $\Phi_1=\Phi_0 3s^{n4}3p^{n5}4s^{n7}4p^{n8}4d^{n9}5s^{n11}5p^{n12}=\Phi^*$; III, $\Phi_1=3d\Phi^*$; IV, $\Phi_1=3d^2\Phi^*$; V, $\Phi_1=3d^3\Phi^*$; VI, $\Phi_1=3d^4\Phi^*$; VII, $\Phi_1=3d^5\Phi^*$; VIII, $\Phi_1=3d^6\Phi^*$; IX, $\Phi_1=3d^7\Phi^*$; X, $\Phi_1=3d^8\Phi^*$; XI, $\Phi_1=3d^9\Phi^*$.

N	I	II	III	IV	V	VI	VII	VIII	IX	X	XI
8	4851										
9	4824	4830									
10	4797	4808	4803								
11	4770	4783	4781	4776							
12	4744	4757	4756	4755	4749						
13	4717	4731	4730	4729	4728	4722					
14	4690	4706	4704	4703	4702	4701	4696				
15	4664	4680	4679	4678	4677	4676	4675	4669			
16	4637	4655	4653	4652	4651	4650	4649	4648	4643		
17	4611	4648	4628	4627	4626	4625	4624	4623	4622	4616	
18		4641	4621	4602	4601	4600	4598	4597	4596	4595	4590
19		4633	4615	4595	4575	4574	4573	4572	4571	4570	4569
20		4625	4606	4588	4569	4549	4548	4547	4546	4545	4544
21		4617	4598	4580	4562	4542	4523	4522	4521	4520	4519
22		4608	4590	4572	4554	4536	4516	4497	4496	4495	4494
23		4600	4582	4564	4546	4528	4510	4490	4471	4470	4469
24		4592	4574	4556	4538	4520	4502	4484	4464	4445	4444
25		4583	4566	4548	4530	4512	4494	4476	4458	4438	4419
26		4574	4557	4540	4522	4504	4486	4468	4450	4432	4412
27		4565	4548	4531	4514	4496	4478	4460	4442	4424	4406
28		4557	4539	4522	4505	4488	4470	4452	4434	4416	4398
29		4548	4530	4513	4496	4479	4462	4444	4426	4408	4390
30		4539	4522	4504	4487	4470	4453	4436	4418	4400	4382
31		4530	4513	4495	4478	4461	4444	4427	4410	4392	4374
32		4521	4504	4487	4469	4452	4435	4418	4401	4384	4366
33		4512	4495	4478	4461	4443	4426	4409	4392	4375	4358
34		4503	4486	4469	4452	4435	4418	4401	4384	4367	4350
35		4500	4477	4460	4443	4426	4409	4392	4375	4358	4341
36		4497	4474	4451	4434	4417	4400	4383	4366	4349	4332
37		4493	4471	4448	4425	4408	4391	4374	4357	4341	4324
38		4489	4467	4445	4422	4400	4383	4366	4349	4332	4315
39		4485	4463	4441	4419	4396	4374	4357	4340	4323	4306
40		4481	4459	4437	4415	4393	4371	4348	4331	4315	4298
41		4477	4455	4433	4411	4389	4367	4345	4323	4306	4289
42		4473	4451	4429	4407	4385	4364	4342	4320	4297	4280
43			4447	4425	4404	4382	4360	4338	4316	4294	4272
44				4422	4400	4378	4356	4334	4312	4291	4269
45					4396	4374	4352	4330	4309	4287	4265
46						4370	4348	4327	4305	4283	4262
47							4344	4323	4301	4279	4258
48								4319	4297	4276	4254
49									4293	4272	4250
50										4268	4246
51											4243

2(c)] we have found a shift of approximately 224 eV. From a comparison of the observed M spectra and the predicted energy values we conclude that a large fraction of initial $2p^k$ core states have survived when the 4-3 radiative deexcitation occurs.

If we use our present knowledge about electron-capture mechanisms at surfaces we can extract the following information from our experimental and theoretical data. Following the classical overbarrier model we find that the neutralization process starts at a critical distance $R_c \cong 130$ Å for Xe^{45+}. The highest n states populated by electron transfer from the copper surface has been estimated by taking the binding energies, the image-charge potential and the work function of Cu into account [31]. We have found a maximum value of approximately $n=43$. On the way in to the surface capture will occur to somewhat lower-n values due to the change of screening and energy-level shifts owing to the increased image charge. We therefore expect a "band" of Rydberg levels to be populated between about $n=20$ and 40 during the approach to the surface. No information exists about the distribution of electrons among those n

TABLE VII. Transition energies (eV) for ions with $Z=54$ (Xe^{47+}) $\Phi_0\Phi_1-2p^{-1}3d\Phi_0\Phi_1$; $\Phi_0=1s^22s^22p^3$; $\Phi_1=3s^{n4}3p^{n5}3d^{n6}4s^{n7}4p^{n8}4d^{n9}5s^{n11}5p^{n12}$; $N=7+n_4+n_5+n_6+n_7+n_8+n_9+n_{11}+n_{12}$; $n_4=1-2$, $n_5=0-6$, $n_7=0-2$, $n_8=0-8$, $n_9=0-10$, $n_{11}=0-2$, $n_{12}=0-6$. I, $\Phi_1=3d^n\Phi_0$, $n=0-9$; II, $\Phi_1=\Phi_03s^{n4}3p^{n5}4s^{n7}4p^{n8}4d^{n9}5s^{n11}5p^{n12}=\Phi^*$; III, $\Phi_1=3d\Phi^*$; IV, $\Phi_1=3d^2\Phi^*$; V, $\Phi_1=3d^3\Phi^*$; VI, $\Phi_1=3d^4\Phi^*$; VII, $\Phi_1=3d^5\Phi^*$; VIII, $\Phi_1=3d^6\Phi^*$; IX, $\Phi_1=3d^7\Phi^*$; X, $\Phi_1=3d^8\Phi^*$; XI, $\Phi_1=3d^9\Phi^*$.

N	I	II	III	IV	V	VI	VII	VIII	IX	X	XI
7	4955										
8	4928	4933									
9	4900	4912	4906								
10	4873	4885	4884	4879							
11	4846	4859	4858	4857	4852						
12	4819	4833	4832	4831	4830	4825					
13	4792	4807	4806	4805	4804	4803	4798				
14	4765	4782	4781	4779	4778	4777	4776	4771			
15	4738	4756	4755	4754	4753	4752	4750	4749	4744		
16	4712	4749	4729	4728	4727	4726	4725	4724	4723	4717	
17		4742	4722	4702	4701	4700	4699	4698	4697	4696	4691
18		4734	4715	4696	4676	4675	4674	4673	4672	4670	4669
19		4726	4707	4689	4669	4649	4648	4647	4646	4645	4644
20		4717	4699	4681	4662	4643	4643	4622	4621	4620	4619
21		4709	4691	4672	4654	4636	4616	4597	4595	4594	4593
22		4701	4683	4664	4646	4628	4609	4590	4570	4569	4568
23		4693	4675	4656	4638	4619	4601	4583	4563	4544	4543
24		4684	4666	4648	4630	4611	4593	4575	4557	4537	4518
25		4675	4657	4640	4622	4603	4585	4567	4549	4531	4511
26		4666	4648	4631	4613	4595	4577	4559	4541	4522	4504
27		4657	4639	4622	4604	4587	4569	4551	4533	4514	4496
28		4648	4630	4613	4596	4578	4561	4543	4525	4506	4488
29		4639	4621	4604	4587	4569	4552	4535	4516	4498	4480
30		4630	4612	4595	4578	4560	4523	4526	4508	4490	4472
31		4621	4604	4586	4569	4551	4534	4517	4500	4482	4464
32		4612	4595	4577	4560	4543	4525	4508	4491	4474	4456
33		4603	4586	4568	4551	4534	4516	4499	4482	4465	4448
34		4600	4577	4559	4542	4525	4508	4490	4473	4456	4439
35		4596	4573	4551	4533	4516	4499	4481	4464	4447	4430
36		4593	4570	4547	4524	4507	4490	4473	4456	4438	4421
37		4589	4566	4544	4521	4498	4481	4464	4447	4430	4413
38		4585	4562	4540	4518	4495	4472	4455	4438	4421	4404
39		4581	4558	4536	4514	4492	4469	4446	4429	4412	4395
40		4577	4554	4532	4510	4488	4466	4443	4420	4403	4386
41		4573	4551	4528	4506	4484	4462	4440	4417	4395	4378
42			4547	4524	4502	4480	4458	4436	4414	4391	4369
43				4520	4498	4476	4454	4432	4410	4388	4366
44					4494	4472	4450	4428	4406	4384	4362
45						4468	4446	4424	4402	4380	4359
46							4442	4420	4398	4377	4355
47								4417	4395	4373	4351
48									4391	4369	4347
49										4365	4343
50											4339

manifolds. The situation is further complicated due to Stark mixing near the surface. In this connection we note that no clear signature of the direct decay of highly excited hollow atom states has been found in the measured x-ray spectra. However, some direct fast radiative transitions from superexcited states with $n \cong 20-40$ may weakly contribute to the high-energy tail above the main M and L x-ray structures. However, these features cannot be resolved with present energy resolution and low beam intensity. This allows the conclusion that the direct population of the $n=3$, 4, and 5 levels occurs in the solid where some fraction of the $n=3$ population comes from cascading via $n=4$ or even $n=5$ states.

The explanation for these pronounced side-feeding mechanisms is the following: For the present projectile beam energy and ion beam-target geometry the approach velocity is about 0.22 a.u. corresponding to 7 Å/fs, which means that the time interval between the first capture events and the ions striking the surface is about 4×10^{-15} sec. This interaction time is much too short for substantial cascading to lower states. Hence the highly excited states consisting of a core of $(1s^2 2s^2 2p^k)$ inner-shell

TABLE VIII. Transition energies (eV) for ions with $Z=54$ (Xe^{48+}) $\Phi_0\Phi_1-2p^{-1}3d\Phi_0\Phi_1$; $\Phi_0=1s^2 2s^2 2p^2$; $\Phi_1=3s^{n4}3p^{n5}3d^{n6}4s^{n7}4p^{n8}4d^{n9}5s^{n11}5p^{n12}$; $N=6+n_4+n_5+n_6+n_7+n_8+n_9+n_{11}+n_{12}$; $n_4=1-2$, $n_5=0-6$, $n_7=0-2$, $n_8=0-8$, $n_9=0-10$, $n_{11}=0-2$, $n_{12}=0-6$; I, $\Phi_1=3d^n\Phi_0$, $n=0-9$; II, $\Phi_1=\Phi_0 3s^{n4}3p^{n5}4s^{n7}4p^{n8}4d^{n9}5s^{n11}5p^{n12}=\Phi^*$; III, $\Phi_1=3d\Phi^*$; IV, $\Phi_1=3d^2\Phi^*$; V, $\Phi_1=3d^3\Phi^*$; VI, $\Phi_1=3d^4\Phi^*$; VII, $\Phi_1=3d^5\Phi^*$; VIII, $\Phi_1=3d^6\Phi^*$; IX, $\Phi_1=3d^7\Phi^*$; X, $\Phi_1=3d^8\Phi^*$; XI, $\Phi_1=3d^9\Phi^*$.

N	I	II	III	IV	V	VI	VII	VIII	IX	X	XI
6	5060										
7	5032	5038									
8	5005	5016	5010								
9	4977	4989	4988	4983							
10	4950	4963	4962	4961	4955						
11	4922	4937	4936	4935	4934	4928					
12	4895	4911	4910	4908	4907	4906	4901				
13	4868	4884	4883	4882	4881	4880	4879	4874			
14	4841	4858	4857	4856	4855	4854	4853	4852	4846		
15	4814	4851	4831	4830	4829	4828	4827	4826	4825	4819	
16		4845	4824	4804	4803	4802	4801	4800	4799	4798	4792
17		4836	4818	4797	4777	4776	4775	4774	4773	4772	4771
18		4828	4809	4791	4771	4751	4750	4749	4747	4746	4745
19		4820	4801	4782	4764	4744	4724	4723	4722	4721	4720
20		4811	4793	4774	4755	4737	4717	4697	4696	4695	4694
21		4803	4784	4766	4747	4729	4710	4690	4671	4670	4669
22		4795	4776	4758	4739	4720	4702	4684	4664	4644	4643
23		4786	4768	4749	4731	4712	4694	4675	4657	4637	4618
24		4777	4759	4741	4723	4704	4686	4667	4649	4631	4611
25		4767	4750	4732	4714	4696	4677	4659	4641	4622	4604
26		4758	4741	4723	4705	4688	4669	4651	4633	4614	4596
27		4749	4732	4714	4696	4679	4661	4643	4624	4606	4588
28		4740	4723	4705	4687	4670	4652	4635	4616	4598	4580
29		4731	4713	4696	4678	4661	4643	4626	4608	4590	4572
30		4722	4704	4687	4669	4652	4634	4617	4599	4582	4564
31		4713	4695	4678	4660	4643	4625	4608	4590	4573	4556
32		4704	4686	4669	4651	4634	4616	4599	4581	4564	4547
33		4701	4677	4660	4642	4625	4607	4590	4573	4555	4538
34		4697	4674	4651	4633	4616	4598	4581	4564	4546	4529
35		4693	4671	4647	4624	4607	4589	4572	4555	4537	4520
36		4689	4667	4644	4621	4598	4581	4563	4546	4529	4511
37		4685	4663	4640	4618	4595	4572	4554	4537	4520	4502
38		4681	4659	4636	4614	4591	4568	4545	4528	4511	4494
39		4677	4655	4632	4610	4587	4565	4542	4519	4502	4485
40		4673	4651	4628	4606	4583	4561	4539	4516	4493	4476
41			4647	4624	4602	4580	4557	4535	4513	4490	4467
42				4620	4598	4576	4553	4531	4509	4487	4464
43					4594	4572	4549	4527	4505	4483	4461
44						4568	4545	4523	4501	4479	4457
45							4541	4519	4497	4475	4453
46								4515	4493	4471	4449
47									4489	4467	4445
48										4463	4441
49											4437

configuration and a band of electrons in $n \cong 20$ to 40 ("hollow atoms") survive until the ions hit the surface.

After the ion has penetrated into the solid, it experiences close binary collisions with Cu target atoms where resonance charge transfer over the barrier (side feeding) can occur. In this way, the M shell can be partially filled by direct electron capture since it is near resonance with the Cu L shell and the critical distance can be estimated to be 0.25 a.u. On the other hand, the $2p$ vacancies of the core survive because the Xe L shell with binding energies around 7961–8719 eV is not resonant with any atomic state in Cu making cross sections for this channel prohibitively small.

V. CONCLUSION

In summary, the observed M and L x rays from Xe ions interacting with a solid surface show remarkable changes in the line intensities and line shifts depending on the varying numbers of L vacancies. The L x-ray lines do not exist if there is no L vacancy initially. The most pronounced L x-ray intensities increase relative to the M

TABLE IX. Transition energies (eV) for ions with $Z=54$ (Xe^{49+}) $\Phi_0\Phi_1-2p^{-1}3d\Phi_0\Phi_1$; $\Phi_0=1s^2 2s^2 2p^2$; $\Phi_1=3s^{n4}3p^{n5}3d^{n6}4s^{n7}4p^{n8}4d^{n9}5s^{n11}5p^{n12}$; $N=5+n_4+n_5+n_6+n_7+n_8+n_9+n_{11}+n_{12}$; $n_4=1-2$, $n_5=0-6$, $n_7=0-2$, $n_8=0-8$, $n_9=0-10$, $n_{11}=0-2$, $n_{12}=0-6$. I, $\Phi_1=3d^n\Phi_0$, $n=0-9$; II, $\Phi_1=\Phi_0 3s^{n4}3p^{n5}4s^{n7}4p^{n8}4d^{n9}5s^{n11}5p^{n12}=\Phi^*$; III, $\Phi_1=3d\Phi^*$; IV, $\Phi_1=3d^2\Phi^*$; V, $\Phi_1=3d^3\Phi^*$; VI, $\Phi_1=3d^4\Phi^*$; VII, $\Phi_1=3d^5\Phi^*$; VIII, $\Phi_1=3d^6\Phi^*$; IX, $\Phi_1=3d^7\Phi^*$; X, $\Phi_1=3d^8\Phi^*$; XI, $\Phi_1=3d^9\Phi^*$.

N	I	II	III	IV	V	VI	VII	VIII	IX	X	XI
5	5166										
6	5138	5144									
7	5110	5121	5116								
8	5082	5095	5094	5088							
9	5055	5068	5067	5066	5060						
10	5027	5041	5040	5039	5038	5033					
11	4999	5015	5014	5013	5012	5011	5005				
12	4972	4988	4987	4986	4985	4984	4983	4977			
13	4944	4962	4961	4960	4959	4958	4957	4956	4950		
14	4917	4955	4935	4934	4933	4932	4930	4929	4928	4923	
15		4948	4928	4907	4906	4905	4904	4903	4902	4901	4895
16		4940	4921	4900	4880	4879	4878	4877	4876	4875	4874
17		4931	4912	4894	4873	4853	4852	4851	4850	4849	4848
18		4923	4904	4885	4866	4846	4826	4825	4824	4823	4822
19		4915	4896	4877	4858	4839	4819	4799	4798	4797	4796
20		4906	4887	4868	4850	4831	4812	4792	4772	4771	4770
21		4898	4879	4860	4841	4823	4804	4785	4765	4745	4744
22		4889	4871	4852	4833	4814	4796	4777	4758	4739	4719
23		4879	4861	4844	4825	4806	4787	4769	4750	4732	4712
24		4870	4852	4834	4817	4798	4779	4761	4742	4724	4705
25		4861	4843	4825	4807	4790	4771	4752	4734	4715	4697
26		4852	4834	4816	4798	4780	4763	4744	4726	4707	4689
27		4843	4825	4807	4789	4771	4754	4736	4717	4699	4680
28		4834	4816	4798	4780	4762	4745	4727	4709	4691	4672
29		4824	4807	4789	4771	4753	4735	4718	4700	4683	4664
30		4815	4797	4780	4762	4744	4726	4709	4691	4674	4656
31		4806	4788	4770	4753	4735	4717	4700	4682	4665	4647
32		4803	4779	4761	4744	4726	4708	4691	4673	4656	4638
33		4799	4776	4752	4735	4717	4699	4682	4664	4647	4629
34		4795	4772	4749	4726	4708	4609	4673	4655	4638	4620
35		4791	4768	4746	4722	4699	4681	4664	4646	4629	4611
36		4787	4764	4742	4719	4696	4672	4655	4637	4620	4602
37		4783	4760	4738	4715	4692	4669	4646	4628	4611	4593
38		4779	4756	4734	4711	4688	4666	4642	4619	4602	4584
39		4775	4752	4730	4707	4684	4662	4639	4616	4593	4575
40			4748	4726	4703	4680	4658	4635	4613	4590	4567
41				4722	4699	4676	4654	4631	4609	4586	4563
42					4695	4672	4650	4627	4605	4582	4560
43						4668	4646	4623	4601	4578	4556
44							4642	4619	4597	4574	4552
45								4615	4593	4571	4548
46									4589	4567	4544
47										4563	4540
48											4536

line intensities and the group of L lines shift to higher energies with increasing number of L vacancies. A comparison of the experimental data with calculated transition energies and rates originating from $n=3-5$ states suggests that transitions of the type $3d$-$2p$ dominate for the L spectra and $4f$-$3d$ for the M line structures, where $4f$ states cannot directly decay to the $2p$ states. In addition, we have also observed weaker transitions arising from $4d$-$2p$ and $5d$-$2p$ as well as $5g$-$4f$.

The discussion of charge-transfer processes and time scales involved when highly charged Xe ions impinge on a Cu surface suggest the following picture: During the approach on the way in to the surface highly excited states ($n \cong 20-40$) are formed. These so-called "hollow atoms" survive until the ions hit the surface. Those ions penetrating into the solid interact with single Cu atoms, leading to a side feeding of $n \geq 3$ states, which give rise to the observed x-ray lines, energies, and intensity ratios.

ACKNOWLEDGMENTS

This work was performed in part under the auspices of the U.S. Department of Energy by Lawrence Livermore National Laboratory under Contract No. W-7405-Eng-48. One of us (R.B.) would like to thank the members of the Institute of Spectroscopy, Russian Academy of Sciences, Troitsk and the Manne Siegbahn Institute of Physics, Stockholm for their hospitality and financial support. We are also indebted to F. Hao and T. Tanaka from the University of Nevada, Reno for stimulating discussions.

APPENDIX

As a representative example the relevant $2p$-$3d$ x-ray energies (Q-$2p^{-1}3dQ$) are given in Tables IV–IX with respect to the number of initial $2p$ vacancies. Thus Table IV shows the energy values in eV for radiative transitions of the type

$$\Phi_0\Phi_1\text{-}2p^{-1}3d\Phi_0\Phi_1 ,$$
$$\Phi_0 = 1s^2 2s^2 2p^6 , \tag{A1}$$
$$\Phi_1 = 3s_4^k 3p_5^k 3d_6^k 4s_7^k 4p_8^k 4d_9^k 5s_{11}^k 5p_{12}^k .$$

This table is divided into I–XI columns, depending on the initial number of electrons in the system. As can be seen in the first column labeled I, the $3d$ subshell becomes progressively filled ($\Phi_1 = 3d^k$). The next column (II) gives the corresponding energy values for Φ_1 with different numbers of electrons in all subshells except $3d$, by occupying first $3s_4^k$, then $3p_5^k$, and so on. Initially, all outer subshells are filled. The columns labeled III–XI are organized in an analogous way, but by progressively adding one $3d$ electron for every new column. The key parameters in our theoretical mode of multiply core-excited states are the occupation numbers k_i; in particular, the number of $2p$ and $3d$ electrons are of primary importance. The data listed in Tables IV–IX clearly indicate that changing the number of $2p$ vacancies by one sifts the L x-ray energies above 100 eV. On the other hand, adding one extra $3d$ electron decreases the energy by about 20–30 eV.

For each L spectrum correlated with a specific $2p$-hole state, i.e.,

$$\Phi_0 = 1s^2 2s^2 2p^k \quad (k = 6 \text{ to } 1) ,$$

350 different $2p$-$3d$ transition energies have been calculated.

*Present address: Department of Physics, University of Nevada, Reno, Reno, NV 89557.

[1] H. J. Andrä, in *Atomic Physics of Highly Charged Ions,* edited by R. Marrus (Plenum, New York, 1989).
[2] D. H. Schneider, M. Clark, B. M. Penetrante, J. McDonald, D. DeWitt, and J. N. Bardsley, Phys. Rev. A **44**, 3119 (1991).
[3] J. P. Briand, L. de Billy, P. Charles, Essabaa, P. Briand, R. Geller, J. P. Desclaux, S. Bliman, and C. Ristori, Phys. Rev. Lett. **65**, 159 (1990).
[4] E. D. Donets, Phys. Scr. **T3**, 11 (1983).
[5] M. Delaunay, S. Dousson, R. Geller, B. Jaquot, D. Hitz, P. Ludwig, P. Sortais, and S. Bliman, Nucl. Instrum. Methods B **23**, 177 (1987).
[6] M. Stöckli, C. L. Cocke, and P. Richard, Rev. Sci. Instrum. **61**, 242 (1990).
[7] F. W. Meyer, J. Phys. (Paris) **50**, C1-263 (1989).
[8] S. T. de Zwart, Nucl. Instrum. Methods B **23**, 239 (1987).
[9] L. Folkerts and R. Morgenstern, in *Atomic Physics of Highly Charged Ions,* edited by E. Salzborn, P. H. Mokler, and A. Müller (Springer, Berlin, 1991); Z. Phys. D **21**, S351 (1991).
[10] H. J. Andrä, A. Simionovici, T. Lamy, A. Brenac, G. Lamboley, S. Andriamonje, J. J. Bonnet, A. Fleury, M. Bonnefoy, M. Chassevent, and A. Pesnelle, in *Atomic Physics of Highly Charged Ions,* edited by E. Salzborn, P. H. Mokler, A. Müller (Springer, Berlin, 1991); Z. Phys. D **21**, S135 (1991).
[11] E. D. Donets, Nucl. Instrum. Methods B **9**, 522 (1985).
[12] D. Schneider, D. DeWitt, M. W. Clark, R. Schuch, C. L. Cocke, R. Schmieder, K. J. Reed, M. H. Chen, R. E. Marrs, M. Levine, and R. Fortner, Phys. Rev. A **42**, 3889 (1990).
[13] C. P. Bhalla, Phys. Rev. A **8**, 2877 (1973); private communication.
[14] E. D. Donets, S. V. Kartashose, and V. P. Ovsyannikov (unpublished).
[15] Y. Conturie, B. Yaakobi, U. Feldman, G. A. Doschek, and R. D. Cowan, J. Opt. Soc. Am. **71**, 1309 (1981).
[16] P. A. Zeijlmans van Emmichoven, C. C. Havener, and F. W. Meyer, Phys. Rev. A **43**, 1405 (1991).
[17] U. I. Safronova, R. Bruch, and D. Schneider, Phys. Scr. (to be published).
[18] S. Salomonson and P. Oster, Phys. Rev. A **41**, 4670 (1990).
[19] S. Salomonson and P. Oster, Phys. Rev. A **40**, 5548 (1989).
[20] E. Lindroth and S. Salomonson, Phys. Rev. A **41**, 4659

(1990).
[21] C. Froese Fischer, *The Hartree-Fock Method for Atoms* (Wiley, New York, 1977).
[22] R. D. Cowan, *The Theory of Atomic Structure and Spectra* (University of California, Berkeley, 1981), and references given therein.
[23] U. I. Safranova, I. Yu. Tolstikhina, R. Bruch, T. Tanaka, F. Hao, and D. Schneider, Phys. Scr. (to be published).
[24] E. V. Aglitskii and U. I. Safronova, *Spectroscopy of Autoionizing States of Atomic Systems* (Energoatomizdat, 1985).
[25] I. A. Ivanov and U. I. Safronova, Opt. Spektrosk. **65**, 5 (1985) [Opt. Spectrosc. **65**, 2 (1988)].
[26] A. V. Vinogradov and U. I. Safronova, Opt. Spektrosk. **52**, 787 (1982) [Opt. Spectrosc. **52**, 471 (1982)].
[27] L. A. Vainshtein, A. V. Vinogradov, I. R. Rublev, and U. I. Safronova, Opt. Spectrosk. **48**, 424 (1980) [Opt. Spectrosc. **48**, 234 (1980)].
[28] U. I. Safronova and V. S. Senashenko, J. Phys. B **14**, 603 (1981).
[29] P. A. Burke and W. Eissner, in *Atoms in Astrophysics,* edited by P. A. Burke, W. B. Eissner, D. A. Hummer, and I. C. Percival (Plenum, New York, 1983), p. 17.
[30] G. Omar and Y. Hahn, Phys. Rev. A **43**, 4695 (1991).
[31] J. Burgdörfer, P. Lerner, and F. Meyer, Phys. Rev. A **44**, 5674 (1991).